Research Article | Vol. 29, No. 22 / 25 Oct 2021 / Optics Express 36111

Optics EXPRESS

Polarization-dependent broadband absorber based on composite metamaterials in the long-wavelength infrared range

HAIHONG YU,[1,2] DEJIA MENG,[3] ZHONGZHU LIANG,[2,3,*] HAIYANG XU,[2] ZHENG QIN,[3] XUEMEI SU,[1] DAVID R. SMITH,[4] AND YICHUN LIU[2]

[1] *Physics College, Jilin University, Changchun 130012, China*
[2] *Center for Advanced Optoelectronic Functional Materials Research and Key Laboratory of UV Light-Emitting Materials and Technology of Ministry of Education, College of Physics, Northeast Normal University, Changchun 130024, China*
[3] *State Key Laboratory of Applied Optics, Changchun Institute of Optics, Fine Mechanics and Physics, Chinese Academy of Science, Changchun, Jilin 130033, China*
[4] *Center for Metamaterials and Integrated Plasmonics, Duke University, P.O. Box 90291, Durham, North Carolina 27708, USA*
[*] *liangzz@nenu.edu.cn*

Abstract: Capturing polarization information has long been an important topic in the field of detection. In this study, two polarization-dependent broadband absorbers based on a composite metamaterial structure were designed and numerically investigated. Unlike in conventional metamaterial absorbers, the bottom metallic film is functionalized to achieve a polarization response or broadband absorption. The simulation results show that the type I absorber exhibits TM polarization-dependent broadband absorption (absorptivity>80%) from 8.37 µm to 12.12 µm. In contrast, the type II absorber presents TE polarization-dependent broadband absorption (absorptivity>80%) from 8.23 µm to 11.93 µm. These devices are extremely sensitive to the change of polarization angle. The absorptivity changes monotonically with an increase of the polarization angle, but it is insensitive to oblique incidence. This design paves the way for realizing broadband polarization-dependent absorption via a simple configuration. It has bright prospects in thermal detection applications and imaging fields.

1. Introduction

The asymmetry in light absorption plays an important role in building a series of optical devices [1]. These devices are of fundamental significance both in thermal detection and image systems [2–4]. However, most of these absorption devices require integration with polarizers and hardly achieve a wide spectral response. The recent rise of metamaterial has attracted much attention due to its designed electromagnetic properties and effects [5]. It can efficiently manipulate the states of light on the nanometer scale and allow the creation of materials with effective values of permittivity and permeability that are not possessed in natural materials [6,7]. Metamaterial absorbers have been demonstrated in applications, such as photodetection [8–10], optical sensing [11–13], energy harvesting [14,15], imaging devices [16–18], etc. As a significant branch, plenty of metamaterial devices have been designed to manipulate the polarization-dependent absorption of electromagnetic waves.

Utilizing asymmetry patterns to achieve polarization-dependent response has been demonstrated, and the grating structure has been proved to be feasible in the literatures [19–21]. Owing to the intrinsic narrow bandwidth of plasmonic resonance, it is convenient to construct

#435579 https://doi.org/10.1364/OE.435579
Journal © 2021 Received 30 Jun 2021; revised 24 Aug 2021; accepted 26 Aug 2021; published 19 Oct 2021

Optics EXPRESS

a narrowband metamaterial perfect absorber. However, a broadband absorption response implies absorbing nearly the entire electromagnetic energy in the target wavelength region, thus improving the utilization efficiency of electromagnetic radiation. Compared with other wave bands, the long-wavelength infrared range has better detection capability when the target is close to the heat source, or when there is stray radiation. It is still quite challenging to obtain a perfect broadband metamaterial absorber using a simple design. There are three main common approaches to realizing broadband absorption by metamaterial absorbers in current research. The first arrangement consists of positioning different elements in a horizontal plane [22,23], the second is placing elements on a multilayer vertically [24,25], and the last method is their welding with lumped elements [26]. However, they all unavoidably increase the complexity of the structure as well as the fabrication. It is feasible to construct broadband absorption using a simple design structure by combining different resonant modes.

In this study, two different types of polarization-dependent broadband absorbers were designed and numerically investigated. Unlike conventional metamaterial absorbers, in the composite metamaterial absorbers, the bottom metallic film is functionalized. It is replaced by a nanostructure to achieve polarization response or broadband absorption. Each layer of the absorber was fully utilized and designed to achieve the desired characteristics. For the type I absorber, the grating structure plays a role in broadband polarization-dependent transmission at the top layer, and the cube is responsible for broadband absorption at the bottom. The absorber exhibits TM polarization-dependent properties. The average absorptivity is over 83.02% in the long-wavelength infrared range (8–12 μm) for TM polarization and as low as 5.22% for TE polarization light. For the type II absorber, the grating structure reflects specific polarized light at the bottom, producing a broadband polarization absorption response at the top. The absorber exhibited TE polarization dependence. The average absorptivity was over 91.98% from 8 μm to 12 μm for TE polarization and only 3.68% for TM polarization. Both absorbers exhibit not only broadband absorption response and highly polarization-dependent properties, but also angle insensitivity under oblique incidence and a simple configuration design. Owing to the multifunctionality of polarization-dependent response and broadband absorption, the absorbers hold potential applications in thermal detection and imaging fields.

2. Results and discussion

To achieve a broadband absorption response, a metamaterial absorber based on a cube nanostructure was proposed and investigated. Figure 1(a) shows the configuration of the unit cell of the metamaterial absorber. The broadband absorber consists of a periodic array of Ti cubes on the top layer, a Ge dielectric layer, and a Ti bottom layer to prevent transmission. The width of the cube is 0.6 μm and the period is 1.4 μm. The thickness of top layer Ti and middle layer Ge is 0.05 μm and 0.35 μm, respectively. The dimensions of the cube and the layer are chosen to satisfy impedance matching condition and excite plasmonic resonance response in the long-wavelength infrared range. The absorption spectrum of the absorber is shown in Fig. 1(b). The material parameters of Ge and Ti were taken from Palik [27] and Ordal [28], respectively. In the simulation, the unit cell was set using periodic boundary conditions along with X and Y directions and perfect matching layer was set along with Z directions. Mesh type was set to auto-optimization gradient meshes. The absorber exhibits polarization-independent broadband absorption with two resonance peaks at 6.05 μm and 9.71 μm, respectively. To reveal the physical mechanism of broadband absorption, the cross section along the $x - z$ plane of the electric field $|E|$ and magnetic field $|H|$ distributions at the resonance wavelengths are presented in Figs. 1(c)–(f). Surface plasmon polaritons are excited at the periphery of the metal cube, which leads to SPP-induced light absorption, as shown in Fig. 1(c) and 1(e). There is an electric field enhancement between adjacent elements, as shown in Fig. 1(c). As for the magnetic field distribution, the propagating surface plasmon (PSP) resonance is excited, as shown in Fig. 1(d). The magnetic field not only localizes in the gap region under the cube, but is also enhanced between adjacent cells. The resonance in Fig. 1(f) is the localized surface plasmon (LSP) mode, where the magnetic field is mainly located in the region between the cube and the Ti bottom layer. The broadband absorption is mainly due to the combination of the LSP and PSP resonance modes.

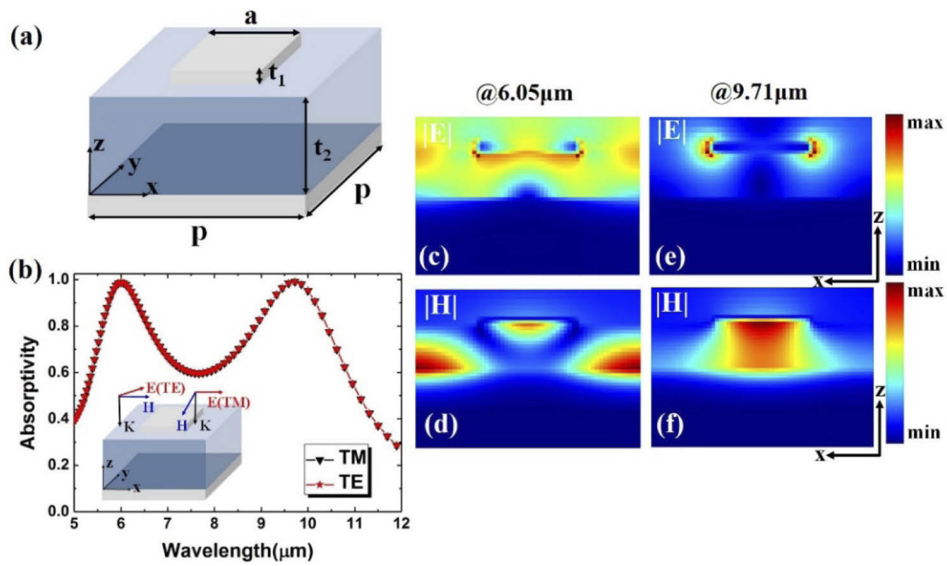

Fig. 1. (a) Three-dimensional schematic of a unit cell of the metamaterial absorber. Ti cube is placed on Ge dielectric layer, and the bottom layer is Ti continuous film. The geometric parameter is p = 1.4 μm, a = 0.6 μm, t_1 = 0.05 μm, t_2 = 0.35 μm. (b) Absorption spectrum for TM and TE polarization under normal incidence. (c)-(f) The distribution of electric field |E| and magnetic field |H| at 6.05 μm and 9.71 μm, respectively.

Although the absorber mentioned above can achieve broadband absorption, it is not polarization-dependent. The asymmetric properties originate from the asymmetry of the pattern, while using the grating structure, in order to realize that the polarization-dependent property is a very effective method. To enhance the transmission property, the grating structure is designed to exhibit dielectric properties in the x-axis direction and metallic properties in the y-axis direction, by adjusting the geometric parameters. Figure 2(a) shows a schematic of the Ti grating on the Ge substrate with a period of 1μm. The width and height of the grating are 0.6μm and 2.15μm, respectively. To exhibit a wider bandwidth and higher transmission, the Fabry–Perot cavity interference effect is enabled when the grating height is approximately one-fourth of the response wavelength. The results show that the grating exhibits broadband transmission in the long-wavelength infrared region for TM polarization light (electric field direction along the x-axis direction) and extremely high reflectivity for TE polarization light (electric field direction along the y-axis direction) in Fig. 2(b). Because Ti is a highly lossy metal, a part of the incident light is absorbed by the grating structure. The broadband polarization response of the grating will be used to construct a polarization-dependent broadband metamaterial absorber in the following section.

The polarization-dependent broadband composite metamaterial absorber is presented in Fig. 3, and it is referred to as the type I absorber. The structure combines the two types of the aforementioned metamaterial structures. It consists of Ti gratings with a width of 0.3 μm and a period of 1.2 μm on the top layer, an ultrathin Ti cube with a width of 0.8 μm on the bottom, and a Ge dielectric layer in the middle. The thicknesses of Ti-Ge-Ti layers from top to bottom are t_1 = 2.05 μm, t_2 = 0.4 μm, and t_3 = 0.05 μm, respectively. To better present the

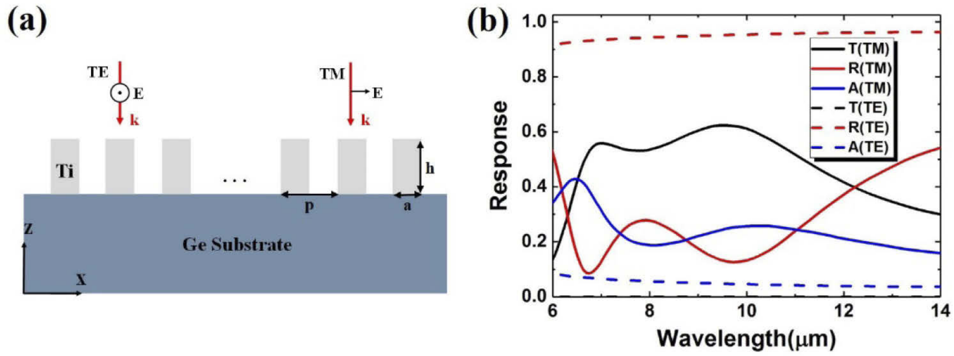

Fig. 2. (a) Ti grating on Ge substrate. (b) Response spectrum lines for TM and TE polarization under normal incidence. The geometric parameter is p = 1 μm, a = 0.6 μm, h = 2.15 μm

structural features, a three-dimensional and cross schematic of a unit cell of the composite metamaterial absorber is presented in Fig. 3(a). The response spectrum lines under the TM and TE polarization incidences are illustrated in Fig. 3(b). The absorptivity can be calculated using the expression$A(\lambda) = 1 - R(\lambda) - T(\lambda)$, where, $A(\lambda)$, $R(\lambda)$ and$T(\lambda)$ represent absorptivity, reflectivity, and transmissivity, respectively. It is observed the absorption device exhibits broadband absorptivity (>80%) from 8.37μm to 12.12μm for TM polarization. The average absorptivity is 91.98% in the long-wavelength infrared range (8–12 μm), whereas it was as low as 5.22% for TE polarization light. The polarization-dependent properties of the absorber are shown in Fig. 3(c). The broadband absorption spectrum under different polarization light and as the angle is increased from 0° to 90° in steps of 15° is shown. The broadband absorption response decreased gradually with an increase in the polarization angle. A novel phenomenon is shown in Fig. 3(d), in which the absorption response and polarization angle show an analogy monotonicity relationship. That is, the absorptivity at resonance wavelengths and average absorptivity (8-12μm) decrease monotonically with an increase in the polarization angle. The proposed absorber exhibited a broadband absorption response and a highly polarization-dependent property.

To gain insight into the mechanism of broadband absorption response, the current density and electromagnetic field profiles on the x–z plane are calculated for the TM polarization incidence. As shown in Fig. 4(a), the electric current distributed in the Ti cube reveals the main origin of the energy loss of broadband absorption. The electric-field intensity is shown in Fig. 4(b). Surface plasmon polaritons (SPPs) are excited in the gratings and cube structure, and light is coupled into the air gap of the grating and localized around the metal corners, which leads to SPP-induced light absorption. The magnetic fields are intrinsically different, as shown in Fig. 4(c). The resonance at 8.79 μm is the PSP resonance in which the magnetic field is strongly confined between the adjacent gratings in Fig. 4(c_1). The incident light was coupled to the PSP wave in the air gaps of the gratings. The distribution of the magnetic field at 11.2 μm is the LSP resonance, and the enhancement is located within the gap between the top gratings and the bottom cube in Fig. 4(c_2). The combination of PSP and LSP resonances lead to a broadband absorption response. The absorptivity of the absorber for the TE wave is extremely low. There is no obvious field enhancement effect under the TE radiation. Therefore, the field distribution of the TE wave is not presented in this paper.

The absorption effect under oblique incidence is an important factor for an effective absorber. The absorption spectra as a function of the incident angle for TM polarization and TE polarization are shown in Fig. 5(a) and Fig. 5(b), respectively. The angle was increased from 0° to 60° in steps of 10°. Furthermore, the designed absorber has stable absorption performance over a wide range

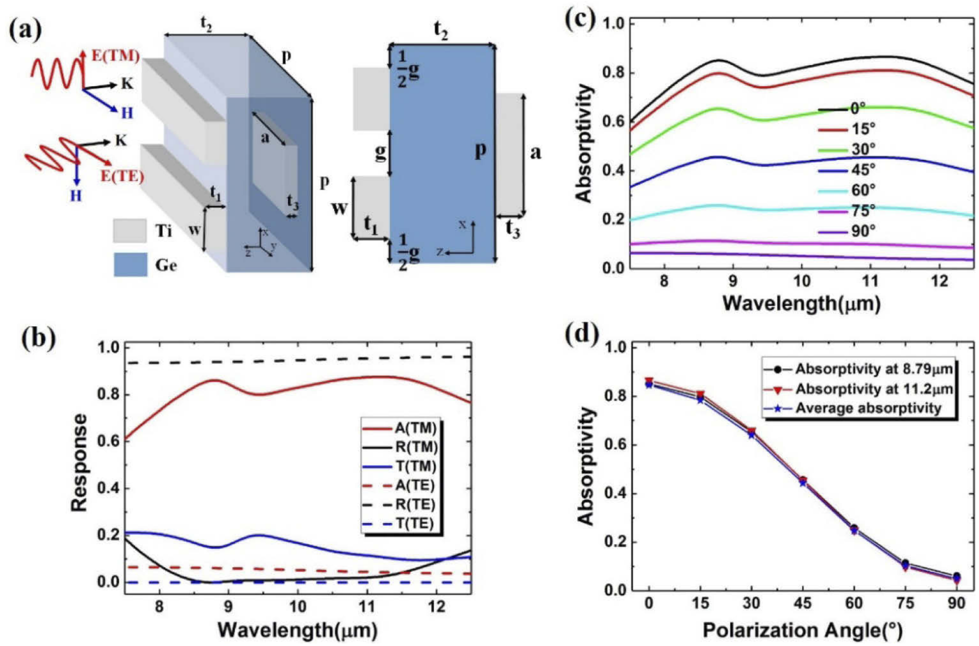

Fig. 3. (a) Three-dimensional and cross schematic diagram of a unit cell of the composite metamaterial absorber. The geometric parameter is p = 1.2 μm, w = 0.3 μm, g = 0.3 μm, a = 0.8 μm, t_1 = 2.05 μm, t_2 = 0.4 μm and t_3 = 0.05 μm. (b) The response spectrum (absorption, reflectivity, and transmission) for TM and TE polarization light. If not particularly emphasized, the absorber is always under normal incidence. (c) The broadband absorption spectrum of different polarization incidence. (d) Absorptivity at resonance wavelengths and average absorptivity in the long-wavelength range as a function of polarization angle, respectively.

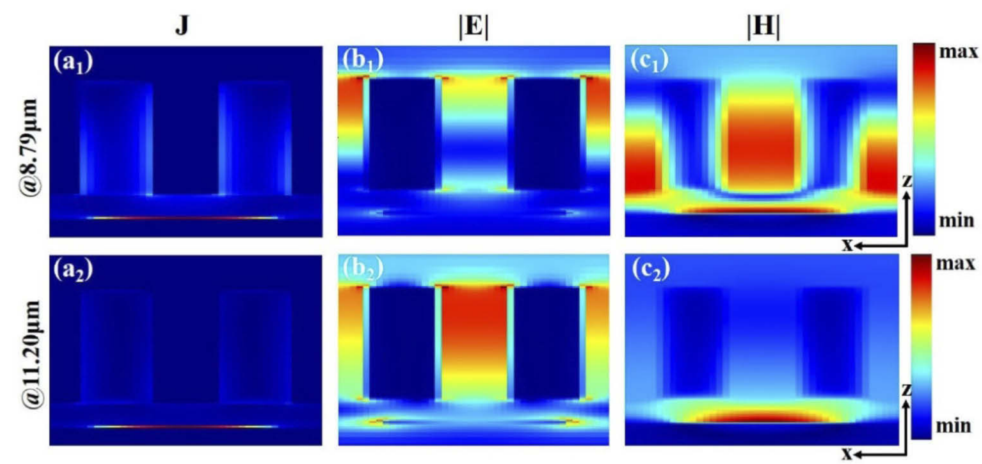

Fig. 4. Current density J and electromagnetic field distributions of type I absorber at resonance wavelengths on the *x–z* plane. The current density J at (a_1)8.79 μm (a_2) 11.20 μm. The distribution of electric field |E| at (b_1)8.79 μm (b_2) 11.20 μm. The distribution of magnetic field |H| at (c_1) 8.79 μm (c_2) 11.20 μm.

of incident angles regardless of being TE or TM radiation. The absorber exhibits angle-insensitive absorption. At an oblique incidence angle of 40°, the absorptivity at resonance wavelengths and average absorptivity (8–12 μm) for TM polarization declined slightly, as shown in Fig. 5(a). One possible reason is the change in the equivalent impedance with oblique incidence. The equivalent impedance in these two modes can be expressed by the following equations [29,30]:

$$\eta_{TM}=\eta \times \cos\theta \tag{1}$$

$$\eta_{TE} = \frac{\eta}{\cos\theta} \tag{2}$$

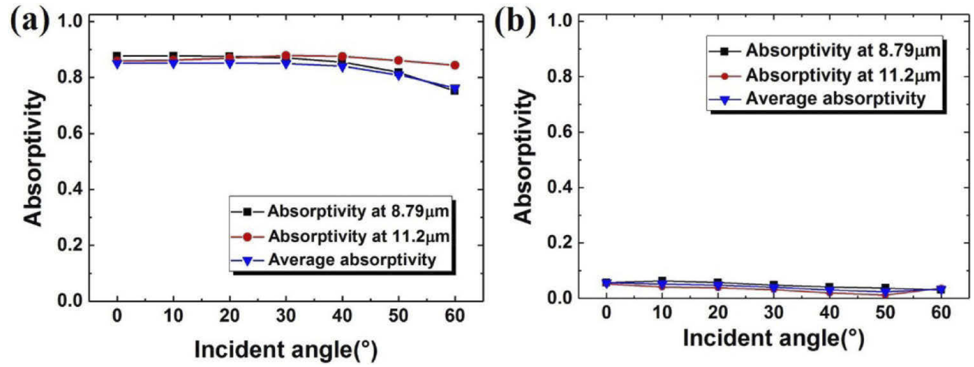

Fig. 5. The absorption spectrum as a function of the incident angle for both (a) TM polarization and (b) TE polarization.

According to Eq. (1), the equivalent impedance in the TM mode slightly declines with an increase in the angle. The equivalent impedance of the absorber exhibits a relative mismatch with the air impedance when the incident angle increases to a certain value, which leads to a change in absorptivity. Almost all TE polarization light is reflected by the absorber configuration, and the absorptivity is extremely low; therefore, the TE mode configuration is excluded from this analysis.

To further improve the absorptivity of the broadband response and polarization-dependent property, another type of polarization-dependent broadband composite absorber was proposed, and the absorber was named type II. A schematic of the structure of its unit cell is shown in Fig. 6(a). It consists of a Ti cube period array on the top layer, a Ti grating period array on the bottom, and a Ge dielectric layer in the middle. The grating array mainly plays a role in achieving polarization-dependent reflection. Thus, the thickness of the grating should be greater than the skin depth of Ti in the target band. The TE polarization light is reflected by the grating array to minimize the transmission. A period array of cubes was utilized to achieve broadband absorption. The response spectrum lines are shown in Fig. 6(b). The absorber presents TE polarization-dependent response and broadband absorption with absorptivity over 80% range from 8.23 μm to 11.93 μm. Because the TE polarization light cannot pass through the grating structure, it is reflected in the composite metamaterial structure. TM radiation can pass through the grating array, and most of it is transmitted and reflected by the metamaterial structure. The average absorptivity is over 91.98% for TE polarization, and it is only 3.68% for TM polarization in the long-wavelength infrared range (8–12 μm). The polarization properties of the absorber under different polarization incidences are shown in Fig. 6(c). The type II absorber exhibits a polarization phenomenon different from that of the type I absorber, in which the absorptivity increases gradually with an increase in the polarization angle. The absorption response and polarization angle show an analogous monotonicity increasing relationship in Fig. 6(d).

Optics EXPRESS

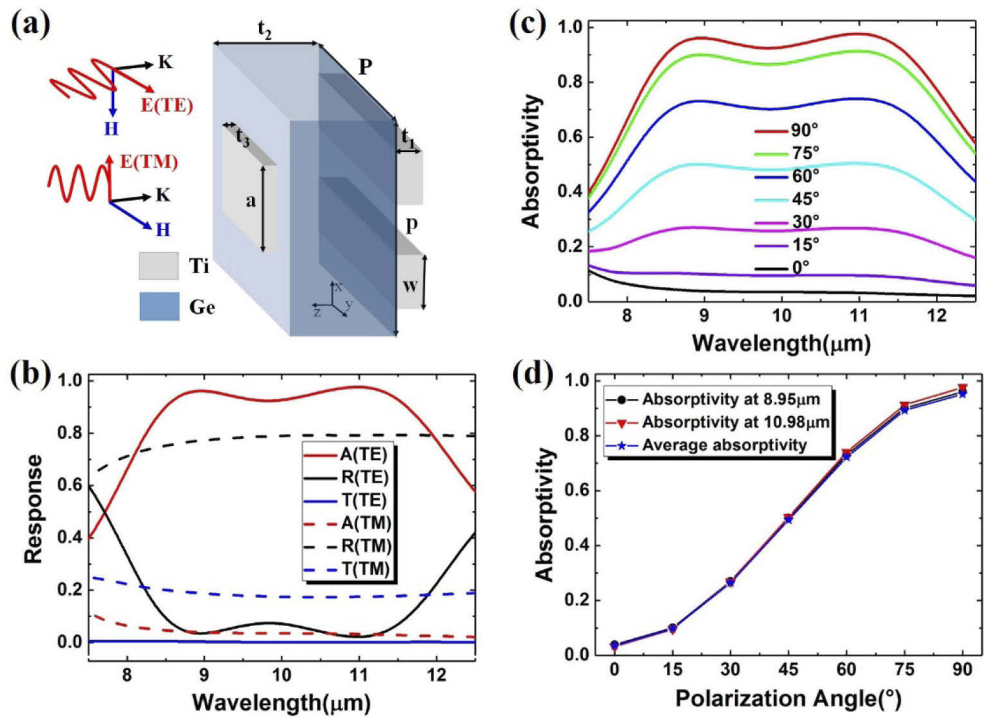

Fig. 6. (a) Three-dimensional schematic of a unit cell of type II metamaterial absorber. The geometric parameter is p = 2.4 µm, w = 0.6 µm, a = 0.7 µm, t_1 = 0.5 µm, t_2 = 0.45 µm and t_3 = 0.05 µm, respectively. (b) The response spectrum under TM and TE polarization light. (c) The broadband absorption spectrum of different polarization incidence. (d) Absorptivity at resonance wavelengths and average absorptivity in the long-wavelength range as a function of polarization angle, respectively.

The electromagnetic field distribution of the type II absorber at resonance wavelengths under TE polarization radiation was calculated to analyze the physical mechanism of the broadband absorption in Fig. 7. The electric field is simulated in the y-z plane, as illustrated in Fig. 7(a) and 7(c). It can be seen from the figure that SPPs are excited around the cube, which leads to SPP-induced light absorption. The magnetic field distributions at the resonance wavelengths are shown in Fig. 7(b) and 7(d). It is also considered to be a PSP resonance at 8.95 µm and a LSP resonance at 10.98 µm. The magnetic field at 8.95 µm is not only enhanced between the adjacent cells but also localized in the gap region underneath the cube, as shown in Fig. 7(a). At a wavelength of 10.79 µm, the LSP resonance dominates the absorption and the enhancement in the gap between the cube and the gratings.

Figure 8 shows the absorption spectrum of the type II absorber under oblique incidence for TM and TE polarization incidences, respectively. The results show that the oblique incidence has little effect on absorption response for TM polarization, and the designed broadband absorber can maintain a high absorption in which absorptivity at resonance wavelengths and average absorptivity are still over 80% when the oblique incidence angle is up to 60° in Fig. 8(a). Similarly, the slight change in absorptivity is also due to the change of equivalent impedance caused by oblique incidence. As for TE polarization, from Fig. 8(b), the absorber shows angle insensitive absorptions, and the absorptivity is independent of incident angle. The results reveal that the proposed absorber still performs fine angle tolerance when the oblique incidence is increased to 60°.

Optics EXPRESS

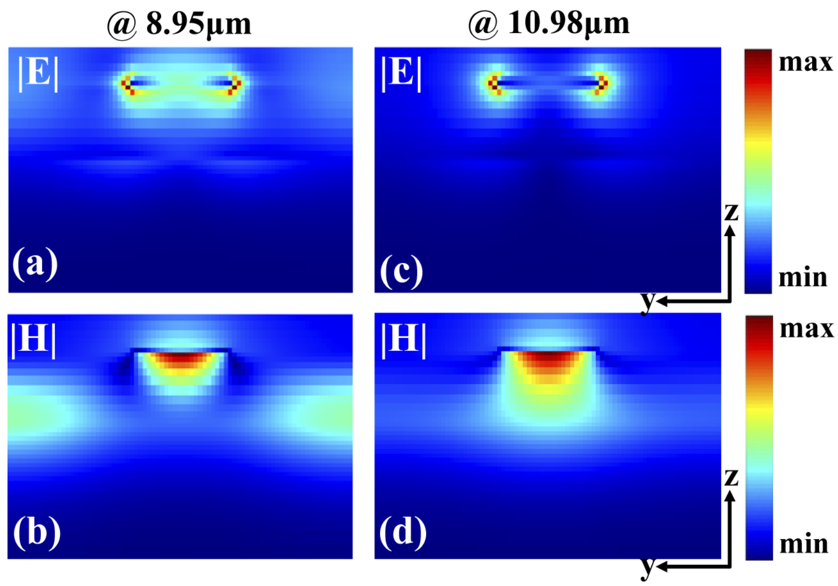

Fig. 7. Electromagnetic field distributions of the type II absorber at resonance wavelengths on the *y*–*z* plane. The distribution of electric field |E| at (a) 8.95 μm (c) 10.98 μm, respectively. The distribution of magnetic field |H| at (b) 8.95 μm (d) 10.98 μm, respectively.

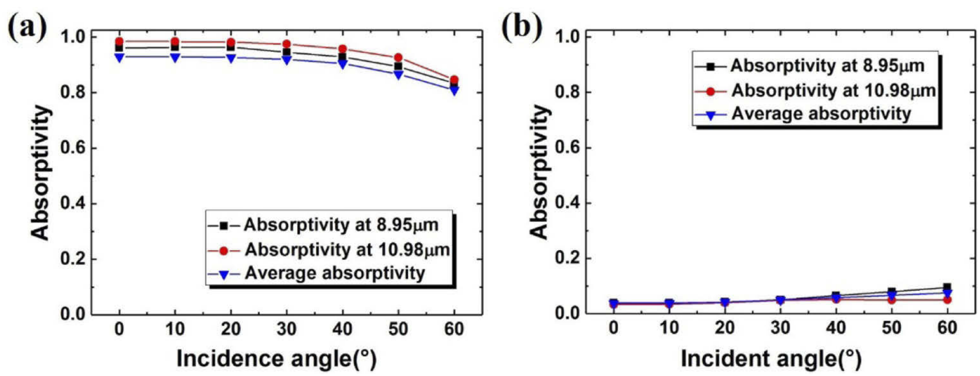

Fig. 8. The absorption spectrum as a function of the incident angle for both (a) TM polarization and (b) TE polarization.

To better illustrate the two different types of metamaterial absorbers, a comparison of the broadband absorption and polarization-dependent properties between type I and type II absorbers are shown in Table 1. The absorbers present different polarization features: type I is TM polarization-dependent and type II is TE polarization-dependent. This is because for type I absorber, the grating structure is located at the top layer and it will reflect TE polarized light and allow TM polarized light to pass through. The absorber only presents high absorption property for TM light. For the type II absorber, the grating structure is located at the bottom layer. TE polarized light cannot pass through the grating structure and can be fully absorbed by the absorber. As for TM polarized light, most of it is reflected and transmitted and rarely absorbed. It can be seen from the table that the polarization property of type II is higher than that of type I, but the bandwidth of type I is greater than that of type II. The two designed metamaterial absorbers show unique absorption characteristics.

Optics EXPRESS

Table 1. Response comparative results between type I and type II metamaterial absorber

Name	Configuration	Material	Response wave band	Response feature	Polarization	Average absorptivity (8–12 μm)	Bandwidth (Absorptivity >80%)
Type I	Grating-dielectric-cube	Ti-Ge-Ti	8–12 μm	TM polarization-dependent	TM	83.02%	3.75 μm
					TE	5.22%	—
Type II	Cube-dielectric-grating	Ti-Ge-Ti	8–12 μm	TE polarization-dependent	TE	91.98%	3.68 μm
					TM	3.68%	—

3. Summary

In conclusion, two polarization-dependent broadband absorbers were demonstrated by utilizing a composite metamaterial design. The grating structure is used to realize a broadband polarized response, whereas the plasmonic cube can excite broadband absorption response. The two devices exhibited significantly different polarized properties. The type I absorber is TM polarization-dependent, and the average absorptivity is over 83.02% for TM polarization and as low as 5.22% for TE polarization in the long-wavelength infrared range. For Type II, the absorber is TE polarization-dependent. Its average absorptivity (8–12 μm) is 91.98% for TE polarization, while it is merely 3.68% for TM polarization. The absorptivity of the two absorbers can be tuned by changing the incidence polarization angle. In the case of oblique incidence, the absorption response exhibits angle-insensitive properties until the angle is increased to 60°. Benefitting from the simple structural design and highly polarization-dependent broadband absorption, the proposed absorbers offer many promising applications in infrared detection and imaging fields.

Funding. CAS President's International Fellowship Initiative (PIFI); Project of CIOMP-Fudan University Collaborative Research; Leading Talents and Team Project of Scientific and Technological Innovation for Young and Middle-aged Groups in Jilin Province (20190101012JH); Excellent Member of Youth Innovation Promotion Association of the Chinese Academy of Sciences (2014193, Y201836); Independent fund of State Kay Laboratory of Applied Optics; Scientific and Technological Development Project of Jilin Province (20190103014JH); National Natural Science Foundation of China (61735018, 61805242).

Disclosures. The authors declare no conflicts of interest.

Data availability. Data underlying the results presented in this paper are not publicly available at this time but may be obtained from the authors upon reasonable request.

References

1. J. M. Zhao, L. Sun, B. Zhu, and Y. J. Feng, "One-way absorber for linearly polarized electromagnetic wave utilizing composite metamaterial," Opt. Express **23**(4), 4658–4665 (2015).
2. S. Ogawa, Y. Takagawa, and M. Kimata, "Broadband polarization-selective uncooled infrared sensors using tapered plasmonic micrograting absorbers," Sens or Actuat A-Phys. **269**, 563–568 (2018).
3. A. Basiri, X. H. Chen, J. Bai, P. Amrollahi, J. Carpenter, Z. Holman, C. Wang, and Y. Yao, "Nature-inspired chiral metasurfaces for circular polarization detection and full-Stokes polarimetric measurements," Light: Sci. Appl. **8**(1), 78 (2019).
4. J. Y. Li, L. Bao, S. Jiang, Q. S. Guo, D. H. Xu, B. Xiong, G. Z. Zhang, and F. Yi, "Inverse design of multifunctional plasmonic metamaterial absorbers for infrared polarimetric imaging," Opt. Express **27**(6), 8375–8386 (2019).
5. F. S. Ma, Y. S. Lin, X. H. Zhang, and C. K. Lee, "Tunable multiband terahertz metamaterials using a reconfigurable electric split-ring resonator array," Light: Sci. Appl. **3**(5), e171 (2014).
6. S. H. Bang, J. Kim, G. Yoon, T. Tanaka, and J. Rho, "Recent Advances in Tunable and Reconfigurable Metamaterials," Micromachines **9**(11), 560 (2018).
7. J. Y. Wang, A. Coillet, O. Demiche, Z. Q. Wang, D. Rego, A. Bouhelier, P. Grelu, and B. Cluze, "Saturable plasmonic metasurfaces for laser mode locking," Light: Sci. Appl. **9**(1), 50 (2020).
8. X. C. Tan, H. Zhang, J. Y. Li, H. W. Wan, Q. S. Guo, H. B. Zhu, H. Liu, and F. Yi, "Non-dispersive infrared multi-gas sensing via nanoantenna integrated narrowband detectors," Nat. Commun. **11**(1), 5245 (2020).

9. J. J. Talghader, A. S. Gawarikar, and R. P. Shea, "Spectral selectivity in infrared thermal detection," Light: Sci. Appl. **1**(8), e24 (2012).
10. X. Liu, T. Tyler, T. Starr, A. F. Starr, N. M. Jokerst, and W. J. Padilla, "Taming the blackbody with infrared metamaterials as selective thermal emitters," Phys. Rev. Lett. **107**(4), 045901 (2011).
11. P. Ginzburg, D. J. Roth, M. E. Nasir, P. Segovia, A. V. Krasavin, J. Levitt, L. M. Hirvonen, B. Wells, K. Suhling, D. Richards, V. A. Podolskiy, and A. V. Zayats, "Spontaneous emission in non-local materials," Light: Sci. Appl. **6**(6), e16273 (2017).
12. X. Fang, K. F. MacDonald, and N. I. Zheludev, "Controlling light with light using coherent metadevices: all-optical transistor, summator and invertor," Light: Sci. Appl. **4**(5), e292 (2015).
13. A. Y. Zhu, F. Yi, J. C. Reed, H. Zhu, and E. Cubukcu, "Optoelectromechanical multimodal biosensor with graphene active region," Nano Lett. **14**(10), 5641–5649 (2014).
14. C. F. Guo, T. Y. Sun, F. Cao, Q. Liu, and Z. F. Ren, "Metallic nanostructures for light trapping in energy-harvesting devices," Light: Sci. Appl. **3**(4), e161 (2014).
15. Z. Y. Xuan, J. Y. Li, Q. Q. Liu, F. Yi, S. W. Wang, and W. Lu, "Artificial Structural Colors and Applications," The Innovation **2**(1), 100081 (2021).
16. D. Wen, F. Yue, G. Li, G. Zheng, K. Chan, S. Chen, M. Chen, K. F. Li, P. W. H. Wong, K. W. Cheah, E. Y. B. Pun, S. Zhang, and X. Chen, "Helicity multiplexed broadband metasurface holograms," Nat. Commun. **6**(1), 8241 (2015).
17. N. Kamaraju, A. Rubano, L. K. Jian, S. Saha, T. Venkatesan, J. Notzold, R. K. Campen, M. Wolf, and T. Kampfrath, "Subcycle control of terahertz waveform polarization using all-optically induced transient metamaterials," Light: Sci. Appl. **3**(2), e155 (2014).
18. B. B. Zeng, Z. Q. Huang, A. Singh, Y. Yao, A. K. Azad, A. D. Mohite, A. J. Taylor, D. R. Smith, and H. T. Chen, "Hybrid graphene metasurfaces for highspeed mid-infrared light modulation and single-pixel imaging," Light: Sci. Appl. **7**(1), 51 (2018).
19. W. Kim, J. P. Guo, and J. Hendrickson, "Subwavelength metal grating metamaterial for polarization-selective optical antireflection coating," J. Opt. Soc. Am. B **32**(7), 1392–1398 (2015).
20. D. M. Nguyen, D. Lee, and J. Rho, "Control of light absorbance using plasmonic grating based perfect absorber at visible and nearinfrared wavelengths," Sci. Rep. **7**(1), 2611 (2017).
21. L. J. Meng, D. Zhao, Q. Li, and M. Qiu, "Polarization-sensitive perfect absorbers at near-infrared wavelengths," Opt. Express **21**(S1), A111–A 122 (2013).
22. Z. G. Li, L. Stan, D. A. Czaplewski, X. D. Yang, and J. Gao, "Wavelength-selective mid-infrared metamaterial absorbers with multiple tungsten cross resonators," Opt. Express **26**(5), 5616–5631 (2018).
23. Z. Q. Liu, G. Q. Liu, X. S. Liu, Y. Wang, and G. L. Fu, "Titanium resonators based ultra-broadband perfect light absorber," Opt Materials **83**, 118–123 (2018).
24. Y. K. Zhong, S. M. Fu, W. M. Huang, D. Rung, J. Y. W. Huang, P. Parashar, and A. Lin, "Polarization-selective ultra-broadband super absorber," Opt. Express **25**(4), A124–A133 (2017).
25. K. Üstün and G. T. Sayan, "Ultra-broadband long-wavelength infrared metamaterial absorber based on a double-layer metasurface structure," J. Opt. Soc. Am. B **34**(2), 456–462 (2017).
26. D. Sood and C. C. Tripathi, "Broadband ultrathin low-profile metamaterial microwave absorber," Appl. Phys. A **124**(12), 837 (2018).
27. E. D. Palik, "Handbook of optical constants of solids," (1985).
28. M. A. Ordal, R. J. Bell, R. W. Alexander, L. L. Long, and M. R. Querry, "Optical properties of fourteen metals in the infrared and far infrared: Al, Co, Cu, Au, Fe, Pb, Mo, Ni, Pd, Pt, Ag, Ti, V, and W," Appl. Opt. **24**(24), 4493–4499 (1985).
29. H. A. Wheeler, "Simple relations derived fom a phased-array antenna made of an infinite current sheet," IEEE Trans. Antennas Propag. **13**(4), 506–514 (1965).
30. M. Li, R. Deng, B. Muneer, and T. Zhang, "Reflection phase modification by metamaterial interface: an understanding of design criteria for ultrathin multispectral absorber," Opt. Express **27**(18), 26131–26142 (2019).